Journal of Computational Acoustics, Vol. 9, No. 2 (2001) 703–718

WAVE PROPAGATION IN 2-D ELASTIC MEDIA USING A SPECTRAL ELEMENT METHOD WITH TRIANGLES AND QUADRANGLES*

DIMITRI KOMATITSCH†
Harvard University, Cambridge, Massachusetts, USA

ROLAND MARTIN
Instituto Mexicano del Petróleo, México D.F., Mexico

JEROEN TROMP†
Harvard University, Cambridge, Massachusetts, USA

MARK A. TAYLOR and BETH A. WINGATE
Los Alamos National Laboratory, Los Alamos, New Mexico, USA

Received 8 October 1999
Revised 25 May 2000

We apply a spectral element method based upon a conforming mesh of quadrangles and triangles to the problem of 2-D elastic wave propagation. The method retains the advantages of classical spectral element methods based upon quadrangles only. It makes use of the classical Gauss–Lobatto–Legendre formulation on the quadrangles, while discretization on the triangles is based upon interpolation at the Fekete points. We obtain a global diagonal mass matrix which allows us to keep the explicit structure of classical spectral element solvers. We demonstrate the accuracy and efficiency of the method by comparing results obtained for pure quadrangle meshes with those obtained using mixed quadrangle-triangle and triangle-only meshes.

1. Introduction

In the context of seismic wave propagation it is important to be able to compute accurate synthetic seismograms using numerical techniques. For more than two decades the most widely used approaches have been the finite difference method[1,2] and the global pseudospectral method.[3,4] Finite difference methods are very popular because of their ease of implementation, but suffer from numerical dispersion and from difficulties related to the implementation of boundary conditions, in particular at the free surface. Pseudospectral methods exhibit very weak numerical dispersion, but instabilites arise in the treatment of boundary conditions and induce difficulties in the time integration scheme.[5] Moreover, due

*Presented at ICTCA'99, the 4th International Conference on Theoretical and Computational Acoustics, May 1999, Trieste, Italy.
†Now at: Seismological Laboratory, California Institute of Technology, Pasadena, California, USA.

to the use of a global polynomial basis, numerical oscillations appear in the presence of strong heterogeneities or sharp boundaries within the model. Classical finite element methods (FEM) circumvent most of these problems, but are based upon low-order approximations and come with high numerical overhead because of the large linear systems involved, particularly in the 3-D case.[6]

In this respect, the spectral element method (SEM), which is based upon a high-order piecewise-polynomial approximation of the weak formulation of the wave equation, has gained significant interest in the seismic modeling community. The classical SEM, which is based on quadrangles in 2-D, and on hexahedra in 3-D, is a high-order method which suffers from very limited numerical dispersion, and the free surface condition is naturally taken into account in the context of the weak formulation.[7,8] In the implementation based on Legendre polynomials the mass matrix is exactly diagonal by construction,[9–12] which results in a drastic reduction in the computational cost, and which enables one to deal with large-scale 3-D structures accurately. Furthermore, complex models that include anisotropy,[13] fluid/solid interfaces[14] or attenuation[12] can be naturally modeled with classical SEMs. The implementation of a SEM on parallel computers based upon the message-passing interface (MPI) is highly efficient,[12,15] which provides a significant advantage over classical pseudospectral approaches.

However, one of the major difficulties associated with the classical SEM is the fact that it is very difficult to mesh realistic geological structures with quadrangles only in 2-D, and even more difficult in 3-D with hexahedra only. This stems from the fact that, for reasons related to accuracy, a good mesh has to honor the main features of a geological structure, such as the main geological interfaces, faults, and velocity contrasts. In this respect, classical FEMs based on triangles in 2-D and on tetrahedra in 3-D are much more flexible.[6] Therefore, in the context of a SEM, it is interesting to introduce more flexibility during the mesh generation step by allowing the use of other types of elements, such as triangles in 2-D or wedges in 3-D, for instance, in regions of steep topography or near basin edges. Similar ideas have previously been used to combine the efficiency of classical techniques, such as finite difference methods, with the flexibility of FEMs.[16] An interesting approach consists of coupling classical SEMs with FEMs based upon triangles using the so-called mortar method.[17,18] This elegant approach allows for a nonconforming matching between spectral element and finite element meshes, but is difficult to implement and increases the numerical cost.

The most popular approach for triangular SEMs has been that developed by Dubiner,[19] Sherwin and Karniadakis[20] and Wingate and Boyd.[21] This method uses a warped tensor product grid within each triangle, designed for the accurate approximation of integrals. It retains the accuracy associated with the SEM on quadrangles and has enabled solutions to problems on mixed meshes. However, unlike the grids used in quadrangles, the warped tensor product grid is oversampled. It requires twice as many points as there are degrees of freedom in the polynomial expansion. This characteristic results in the loss of the diagonal mass matrix.

An alternative approach is to use critically sampled points in the triangle designed for accurate approximation rather than for integration, such as the Fekete points.[22,23] These

points are a natural generalization of the points used by the SEM on quadrangles. They enable a conforming matching between triangles and quadrangles while keeping the important properties of classical SEMs, including the diagonal mass matrix.[24]

The purpose of this paper is to apply the Fekete point technique to the problem of 2-D elastic wave propagation. We illustrate the accuracy of the method by comparing the results obtained for the case of a homogeneous medium using a mesh of quadrangles only with those obtained using a mixed mesh, as well as a mesh of triangles only. Detailed comparisons to the analytical solution are presented and demonstrate that triangles are only slightly less accurate than quadrangles of the same size. For a polynomial degree $N = 5$, good accuracy is obtained with quadrangles using roughly 4.5 points per wavelength, while triangles require roughly 6 points per wavelength to reach a similar level of precision.

2. Elastic Wave Equation

In a heterogeneous elastic medium, the linear wave equation may be written as

$$\rho \ddot{\mathbf{u}} = \nabla \cdot \boldsymbol{\sigma} + \mathbf{f}\,, \tag{2.1}$$

where $\mathbf{u}$ denotes the displacement vector, $\boldsymbol{\sigma}$ the symmetric stress tensor, ρ the density, and $\mathbf{f}$ an external force. A dot over a symbol denotes time differentiation. Even though the SEM can deal with fully anisotropic media[13] and with elastic media with fluid regions,[14] for simplicity we will restrict ourselves to linear elastic isotropic media. In that case, Hooke's law relating components of strain $\varepsilon_{ij} = (\partial_i u_j + \partial_j u_i)/2$ to those of stress σ_{ij} reduces to $\sigma_{ij} = \lambda \delta_{ij} \varepsilon_{kk} + 2\mu \varepsilon_{ij}$, where λ and μ are the two Lamé parameters, and where δ_{ij} denotes the Kronecker delta. In the case of a medium with free surfaces, e.g., the surface of the Earth, the boundary condition is zero traction at the surface: $\boldsymbol{\sigma} \cdot \hat{\mathbf{n}} = \mathbf{0}$, where $\hat{\mathbf{n}}$ is the unit outward normal vector.

3. Classical Spectral Elements on Quadrangles

In a spectral element approach, the strong form of the equations of motion (2.1) is first rewritten in a variational or weak formulation. This is accomplished by dotting it with an arbitrary test vector $\mathbf{w}$ and integrating by parts over the region of interest,[25] which gives

$$\int_\Omega \rho \mathbf{w} \cdot \ddot{\mathbf{u}}\, \mathrm{d}\Omega + \int_\Omega \boldsymbol{\nabla} \mathbf{w} : \boldsymbol{\sigma}\, \mathrm{d}\Omega = \int_\Omega \mathbf{w} \cdot \mathbf{f}\, \mathrm{d}\Omega\,. \tag{3.1}$$

Here Ω denotes the physical region of interest. A colon denotes the tensor product. In the integration by parts, we have used the fact that the traction vanishes on the free boundaries of the domain.

The classical Legendre spectral element discretization of problem (3.1) based upon quadrangles proceeds as follows: a conforming mesh of n_{el} nonoverlapping quadrangles Ω_e is defined on the domain Ω, as in a classical FEM. These elements are subsequently mapped individually to a reference square $\Lambda = [-1, 1] \times [-1, 1]$ using an invertible local mapping $\mathcal{F}_e : \Lambda \to \Omega_e$, which enables one to go from the physical domain to the reference domain, and vice versa.

On the reference square Λ, we introduce a set of local basis functions consisting of polynomials of degree N. On each element Ω_e, mapped to the reference square Λ, we define a set of nodes and choose the polynomial approximations $\mathbf{u}_N^e$ and $\mathbf{w}_N^e$ of $\mathbf{u}$ and $\mathbf{w}$ to be the Lagrange interpolants on this set of nodes. These nodes, $\xi_p \in [-1,1]$, $p \in 0,\ldots,N$, are the Gauss–Lobatto–Legendre (GLL) points, which are the $N+1$ roots of $(1-\xi^2)P'_N(\xi) = 0$, where $P'_N(\xi)$ is the derivative of the Legendre polynomial of degree N. They can be computed numerically.[26] On the reference square Λ, the restriction of a given function u_N to the element Ω_e can be expressed using a product of 1-D Lagrange interpolants, a property that is often referred to as the tensorisation of the basis:

$$u_N^e(\xi,\eta) = \sum_{p=0}^{N}\sum_{q=0}^{N} u_N^e(\xi_p,\eta_q)h_p(\xi)h_q(\eta)\,. \tag{3.2}$$

Here $h_p(\xi)$ denotes the p-th 1-D Lagrange interpolant at the $(N+1)$ GLL points introduced above, which is by definition the unique polynomial of degree N that is equal to one at $\xi = \xi_p$ and to zero at all other points $\xi = \xi_q$ for which $q \neq p$. From this definition we obtain the fundamental property:

$$h_p(\xi_q) = \delta_{pq}\,. \tag{3.3}$$

Once we have invoked the piecewise-polynomial approximation (3.2), the integrals in (3.1) can be approximated at the elemental level using the GLL integration rule:

$$\int_\Omega u_N w_N \,\mathrm{d}\Omega = \sum_{e=1}^{n_{el}}\int_{\Omega_e} u_N^e w_N^e \,\mathrm{d}\Omega \simeq \sum_{e=1}^{n_{el}}\sum_{p=0}^{N}\omega_p\sum_{q=0}^{N}\omega_q J_e(\xi_p,\eta_q)u_N^e(\xi_p,\eta_q)w_N^e(\xi_p,\eta_q)\,. \tag{3.4}$$

The quadrature weights $\omega_p > 0$, which are independent of the element, are determined numerically,[26] and J_e is the Jacobian associated with the mapping $\mathcal{F}_e$ from the element Ω_e to the reference square Λ. Gradients are first computed on the reference square Λ:

$$\begin{aligned}\partial_\xi u_N^e(\xi,\eta) &= \sum_{p=0}^{N}\sum_{q=0}^{N} u_N^e(\xi_p,\eta_q)h'_p(\xi)h_q(\eta)\\ \text{and}\quad \partial_\eta u_N^e(\xi,\eta) &= \sum_{p=0}^{N}\sum_{q=0}^{N} u_N^e(\xi_p,\eta_q)h_p(\xi)h'_q(\eta)\,,\end{aligned} \tag{3.5}$$

where h' denotes the derivative of the 1-D Lagrange interpolant, which is calculated analytically. We subsequently use the chain rule to compute the derivatives in the physical domain, the components of the Jacobian matrix being computed based upon the mapping $\mathcal{F}_e$. Because of the tensorisation, when evaluating the gradient at any of the GLL points (ξ_i,η_j) of the local mesh, using definition (3.3) of the Lagrange interpolants, Eq. (3.5) reduces to:

$$\partial_\xi u_N^e(\xi_i,\eta_j) = \sum_{p=0}^{N} u_N^e(\xi_p,\eta_j)h'_p(\xi_i) \quad\text{and}\quad \partial_\eta u_N^e(\xi_i,\eta_j) = \sum_{q=0}^{N} u_N^e(\xi_i,\eta_q)h'_q(\eta_j)\,. \tag{3.6}$$

Therefore the cost for computing a derivative is exactly $N + 1$ multiplications and N additions, for a total of $2N + 1$ operations.

After this spatial discretization with spectral elements, imposing that the variational formulation holds for any test vector $\mathbf{w}$, as in a classical FEM, we have to solve an ordinary differential equation in time. Denoting by U the global vector of unknown displacement in the medium, this system can be written in matrix form as

$$M\ddot{U} + KU = F\,, \tag{3.7}$$

where M is the mass matrix, K the stiffness matrix, and F the source term. As mentioned previously, a very important property of the Legendre SEM, which allows for drastic reductions in the complexity and cost of the algorithm, is the fact that the mass matrix M is exactly diagonal by construction as a consequence of the choice of Lagrange interpolants at the GLL points in conjunction with the GLL integration rule. This constitutes a major difference compared to classical FEMs.[11,12]

To take full advantage of this property, discretization of the second-order ordinary differential equation in time (3.7) is achieved using a classical explicit Newmark scheme,[25] which is second-order accurate and conditionally stable. Usually a force source is considered, as in Eq. (2.1), and zero initial displacement and velocity are assumed throughout the model.

4. Spectral Elements on Triangles

The natural extension of the diagonal-mass-matrix spectral element method to triangles would be to use GLL points in each triangle. Unfortunately, in the general case it is not known if such points exist, and if so, constructing them numerically turns out to be an extremely hard problem. There are a few, low-degree special cases, but there are also degrees for which it is known that such quadrature formulas do not exist. Many of these results for the triangle are summarized in Lyness and Cools.[27] Gaussian (and Gauss–Lobatto) type quadrature formulas seem to be extremely rare and restricted to a few domains like the $[-1, 1]$ interval and its tensor products.

An alternative to the GLL points in the triangle is to choose points optimized for their interpolation and approximation properties, rather than quadrature. Recent work in this area includes the Fekete points, mean-L_2 points, and minimum energy electrostatic points.[22,28,23] These points are the solutions to extremal problems and must be computed numerically, but in most cases the minimization is a much more tractable problem than computing optimal quadrature points. All of these points have natural extensions to three dimensions. They have been computed for the tetrahedron,[29,30] and in wedges one would use a tensor product of Fekete points in the triangle with the GLL points in the third direction.

For the SEM, we choose the Fekete points over other possible interpolation points for the following reasons:

- On the $[-1, 1]$ interval in the 1-D case, Fekete points are the GLL points.[31]
- On the square, Fekete points have recently been shown to be the tensor product of the GLL points.[32] Thus the conventional SEM can also be considered a Fekete point SEM.

- Under suitable assumptions, one can show that the Fekete points along each edge of the triangle are the GLL points.[33] This has been verified numerically up to degree $N = 19$ in Taylor and Wingate.[23] Thus the Fekete points provide a natural coupling with a SEM on quadrangles.
- Fekete points have near-optimal interpolation properties, and for degrees $N > 9$ they are the best interpolation points known for the triangle.[23]

The Fekete points (and other near-optimal interpolation points) are defined relative to a finite-dimensional space of functions from which the interpolants are constructed. Thus one must first determine the correct functional space for the SEM. Usually, the functional spaces for high-order finite elements are built based upon polynomials. As mentioned in the previous section, the SEM for quadrangles uses a tensor product of Lagrange interpolating polynomials. Their span is the space of polynomials in ξ and η which have a maximum degree in ξ or η of at most N. For the triangle, the most natural and commonly used polynomial space is the set of two-dimensional polynomials in ξ and η with a total degree of at most N. This space has dimension $N_t = (N+1)(N+2)/2$, and thus in order to construct interpolating polynomials we need exactly N_t points.

Once the polynomial space is chosen, the N_t Fekete points are defined in terms of a generalized Vandermonde matrix V (e.g., Ref. 34). Let $\{D_p\}$, $p = 1, \ldots, N_t$, be any basis for the set of polynomials with degree of at most N. Let $\{(\xi_p, \eta_p)\}$ be a set of points in the right triangle of base $[-1, 1]$ and height $[-1, 1]$. The (q, p) component of the Vandermonde matrix is $D_q(\xi_p, \eta_p)$. The Fekete points are those which maximize the determinant of the Vandermonde matrix, $|V|$, where the maximum is taken over all possible sets of points in the triangle. Fekete points are independent of our choice of basis, since any change of basis only multiplies the determinant by a constant independent of the points. However, in practice for numerical computations it is very important to use a well conditioned orthogonal basis for the triangle. Maximizing $|V|$ makes this matrix far from singular.

According to Bos,[32] there is a maximum number of points lying on the boundary, and they are exactly the 1-D GLL points. Therefore, the Fekete triangular elements naturally conform with the classical quadrilateral elements. In order to have a suitable orthogonal basis in the triangular polynomial truncation space given above, we use the Dubiner polynomials.[19] The matrix V can then be thought of as the inverse of the Dubiner transform matrix, and maps Dubiner coefficients of a function into the grid-point values of that function at (ξ_p, η_p). A stable procedure for performing the maximization using the steepest descent algorithm is given in Taylor and Wingate.[23] This approach is extremely sensitive to the initial conditions. The best initial guess for the point distribution turns out to be the set of points generating a density approximating the extremal measure for the triangle given in Baran.[35] The Fekete points (ξ_p, η_p) for the case $N = 5$ are illustrated in Fig. 1.

From the definition of the Fekete points, it can be shown that the Lagrange interpolating polynomials are bounded by 1 inside the triangle, and thus achieve their maximum at these points. This property is also shared by the interpolants at the GLL points, since they are the Fekete points for the square. This bound can then be used to derive classical bounds

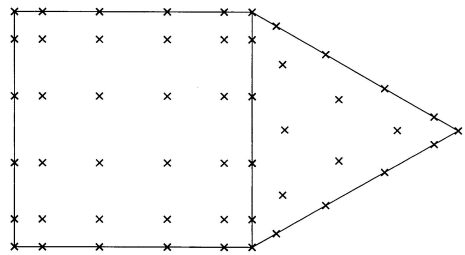

Fig. 1. Equilateral triangle showing the $(N+1)(N+2)/2 = 21$ Fekete points for the case of a polynomial degree $N = 5$, and quadrangle showing the $(N+1)^2 = 36$ Gauss-Lobatto-Legendre points. The Fekete points on the edge of the triangle and the Gauss-Lobatto-Legendre points on the edge of the quadrangle exactly match in the global mesh. There are $N + 1 = 6$ points on the common edge.

on interpolation, differentiation and integration, which show that the Fekete points are well suited for all these tasks. In general, other point sets will generate interpolants which are not bounded by 1. Poorly chosen interpolation points are unusable in a numerical method because their interpolating polynomials have strong oscillations between the points.

To use Fekete points in the SEM, we need to compute the Lagrange interpolants and their derivatives. The most convenient way of doing this is to expand the interpolants in terms of Dubiner polynomials:

$$\Phi_p(\xi,\eta) = \sum_{j=1}^{N_t} a_j^p D_j(\xi,\eta)\,. \tag{4.1}$$

The coefficients of the Dubiner expansion a_j^p are given by the (p,j) elements of the inverse Vandermonde matrix. To compute these coefficients, the Vandermonde matrix is inverted numerically. The derivatives of the Lagrange interpolants are then given by

$$\partial_\xi \Phi_p(\xi,\eta) = \sum_{j=1}^{N_t} a_j^p \partial_\xi D_j(\xi,\eta) \quad \text{and} \quad \partial_\eta \Phi_p(\xi,\eta) = \sum_{j=1}^{N_t} a_j^p \partial_\eta D_j(\xi,\eta)\,, \tag{4.2}$$

since the partial derivatives of the Dubiner polynomials are known analytically. These values are computed once and for all and stored for use by the SEM.

The displacement field and the test functions are then expressed at the element level just as in the case with quadrangles. Using the N_t interpolation functions Φ_p, we write:

$$u_N^e(\xi,\eta) = \sum_{p=1}^{N_t} u_N^e(\xi_p,\eta_p)\Phi_p(\xi,\eta)\,. \tag{4.3}$$

Their partial derivatives are obtained by analytically differentiating the Φ_p:

$$\partial_\xi u_N^e(\xi,\eta) = \sum_{p=1}^{N_t} u_N^e(\xi_p,\eta_p)\partial_\xi \Phi_p(\xi,\eta) \quad \text{and} \quad \partial_\eta u_N^e(\xi,\eta) = \sum_{p=1}^{N_t} u_N^e(\xi_p,\eta_p)\partial_\eta \Phi_p(\xi,\eta)\,. \tag{4.4}$$

These derivatives can be evaluated at the N_t Fekete points (ξ_q, η_q) based upon knowledge of the two $N_t \times N_t$ derivation matrices $\partial_\xi \Phi_p(\xi_q, \eta_q)$ and $\partial_\eta \Phi_p(\xi_q, \eta_q)$. We see from Eq. (4.4) that the cost of calculating a derivative is exactly N_t multiplications and $N_t - 1$ additions, for a total of $2N_t - 1 = (N+1)(N+2) - 1$ operations. Relative to the case of quadrangles detailed in the previous section, we have lost the so-called tensorisation of the basis.

To evaluate the integrals needed in the SEM, we use a procedure similar to that used in quadrangles. Within each triangular element Ω_e, we have:

$$\int_{\Omega_e} u_N^e w_N^e \, \mathrm{d}\Omega \simeq \sum_{p=1}^{N_t} \omega_p J_e(\xi_p, \eta_p) u_N^e(\xi_p, \eta_p) w_N^e(\xi_p, \eta_p) \,. \tag{4.5}$$

The quadrature weights ω_p are determined in the same fashion as for the classical GLL points, i.e., they are the only set of weights which integrate exactly all the basis functions of degree N. For the triangle, the pth weight is given by the first Dubiner coefficient of the p-th interpolating polynomial.

As mentioned above, the Fekete points exactly correspond to the GLL points on the three edges of the triangle. Therefore, as illustrated in Fig. 1, for a given geological structure, mixed unstructured meshes, composed of both quadrangles and triangles in which the points on the edges of both types of elements match exactly, can be constructed. In this fashion, high flexibility can be attained during the mesh generation phase for complex geological structures, thus reducing the difficulties of mesh creation based upon quadrangles only. Let us mention that many powerful meshing tools exist for that purpose in the finite-element community, which can be used directly to create mixed meshes for the SEM.

Since all the points match on the common edge between a quadrangle and a triangle, and since the same polynomial degree is used for the approximation on both elements, the continuity of the field is ensured everywhere on the common edge. Therefore, the contributions to the global system, computed separately for both elements, can be assembled in the same manner as in the classical SEM based upon quadrangles. The global mass matrix for a mixed mesh remains diagonal since the elementary mass matrices are diagonal for both types of elements. Thus, the very efficient structure of classical spectral-element solvers is preserved, in particular the high efficiency on parallel computers,[12] and the new type of element is easily embedded in an existing spectral-element solver. The main difference introduced by the triangular elements is that, on a triangle, the tensorisation of the classical quadrangular spectral elements is lost, and therefore the cost of computing a derivative on a triangle is $(N+1)(N+2) - 1$, whereas it is only $2N + 1$ on a quadrangle. Thus, from the point of view of computations, triangles are more expensive than quadrangles in a ratio $R = [(N+1)(N+2) - 1]/(2N+1) \simeq N/2$, the latter approximation being valid for large N. However, in wave propagation problems the polynomial degree N always remains small, typically between five and eight,[10–12] and therefore this increase in CPU cost will be reasonable in practical situations, particularly if the mesh is mainly composed of quadrangles, with a few triangles. This additional cost would be more significant in the case of 3-D elements such as wedges or tetrahedra.

5. Numerical Validation

In order to validate the method, to demonstrate its efficiency, and estimate its accuracy with respect to classical SEMs based upon quadrangles, we consider a 2-D homogeneous test case consisting of a block of size 2400 m $\times$ 2400 m, with P-wave velocity $c_p = 3200$ m/s, S-wave velocity $c_s = 1847.5$ m/s, and density $\rho = 2200$ kg/m^3. The source is a vertical force placed exactly in the middle of the model at $x_s = 1200$ m and $z_s = 1200$ m. To study the dispersion of waves traveling through the grid several times, we use periodic conditions on all the sides of the model, thus simulating an infinite medium with a network of identical sources periodically repeated along the horizontal and vertical directions. The analytical solution for such a problem can be computed by summing the contributions of all the individual sources calculated based upon the Green's function of the medium[36]; this analytical solution will be used as a reference in what follows.

We first use a classical SEM based upon quadrangles only. The regular mesh consists of 48×48 spectral elements of size 50 m $\times$ 50 m. A polynomial degree $N = 5$ is used within each element, and therefore the global grid contains $(48 \times 5 + 1)^2 = 58081$ points. Using a classical SEM with $N = 5$ the minimum number of grid points per wavelength required for an accurate simulation is roughly five.[12] Therefore, we select for the time dependence of the source a Ricker wavelet, i.e., the second derivative of a Gaussian, with dominant frequency $f_0 = 16$ Hz and onset time $t_0 = 0.07$ s. This gives a mean value of 4.6 points per S-wavelength at the highest frequency $f_{\max}$ at which the Ricker wavelet has some significant energy, which is $f_{\max} \simeq 2.5 f_0$. Since the GLL points are not evenly spaced, it is not possible to define a uniform number of points per wavelength, and the mean value given here is computed by averaging over an element, i.e., computing the number of elements per wavelength and dividing by $N + 1$, the number of points per element, as if they were evenly spaced.

We purposely choose a small time-step Δt in order to ensure that the contribution of the finite-difference time scheme to the global numerical error is small in the comparisons between the spectral element results and the analytical solution, since we want to focus on validating the spatial discretization. We therefore use $\Delta t = 0.5$ ms and we propagate the signal for 2 s, i.e., a total of 4000 time-steps. Such a value of the time-step also verifies the Courant stability condition of the explicit Newmark scheme. Since the time scheme we use is only second-order accurate, it might in the future be of interest to use higher-order schemes[37] to be consistent with the high-order spatial discretization used in the SEM.

Figure 2 shows the two components of the displacement vector recorded at a receiver located at $x_r = 2000$ m and $z_r = 2000$ m, a distance of 1131.4 m from the source. We clearly observe the direct P-wave (around $t = 0.4$ s) and direct S-wave (around $t = 0.6$ s) generated by the source, as well as similar waves that have traveled two, three or four times through the grid (after $t = 0.65$ s) because of the periodic conditions. In order to estimate the accuracy of the classical SEM for this test case we also present the analytical solution. Since the two curves are almost superimposed, we plot the difference (residual) between them amplified by a factor of five for clarity. The overall agreement is excellent, illustrating that the classical SEM is highly accurate. The residual is larger for the S-wave around $t = 0.6$ s

than for the P-wave around $t = 0.4$ s, as expected, since the S-wavelength is shorter than the P-wavelength and thus sampled by fewer grid points. The residual slightly increases with time, because of the accumulated dispersion error for waves that have traveled several times through the grid. Next, we wish to validate the SEM for triangles and estimate its accuracy. We therefore redo exactly the same simulation, but first using a mixed mesh of quadrangles with four lines of triangles, and subsequently using a mesh of triangles only. In order to be

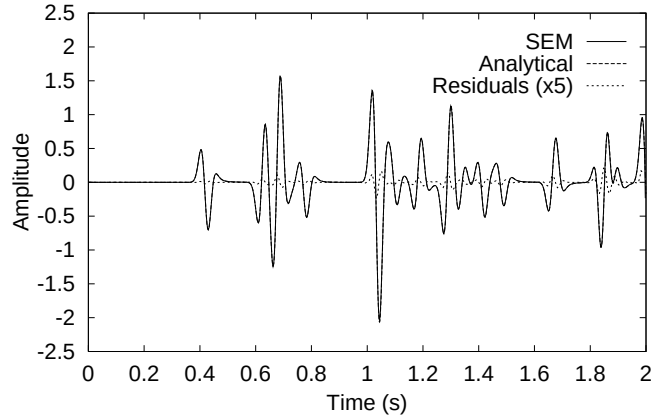

(a)

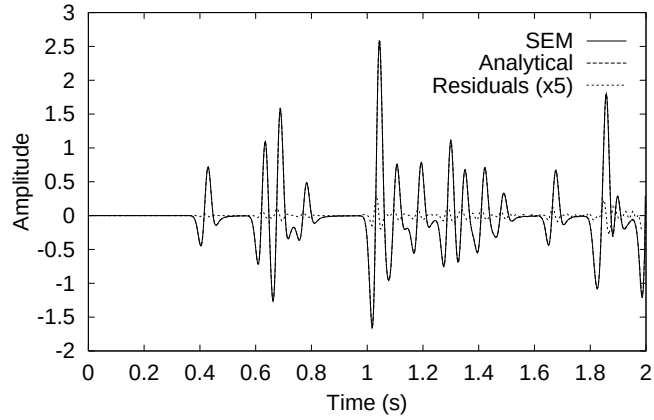

(b)

Fig. 2. Horizontal (a) and vertical (b) component of displacement (solid line) recorded at a receiver located at $x_r = 2000$ m and $z_r = 2000$ m, for a 2400 m $\times$ 2400 m block with a vertical force source located in its middle, at $x_s = 1200$ m and $z_s = 1200$ m. The distance between the source and the receiver is 1131.4 m. The dominant frequency of the Ricker source is $f_0 = 16$ Hz. The medium is discretized using 48×48 classical quadrangular spectral elements, with a polynomial degree $N = 5$. The direct P-wave (around $t = 0.4$ s) and direct S-wave (around $t = 0.6$ s) can be clearly observed, as well as similar waves that have traveled several times through the grid because of the periodic conditions (after $t = 0.65$ s). The analytical solution is also presented (dashed line), as well as the residuals between the two curves amplified by a factor of five for clarity (dotted line). The numerical and analytical solutions are in excellent agreement.

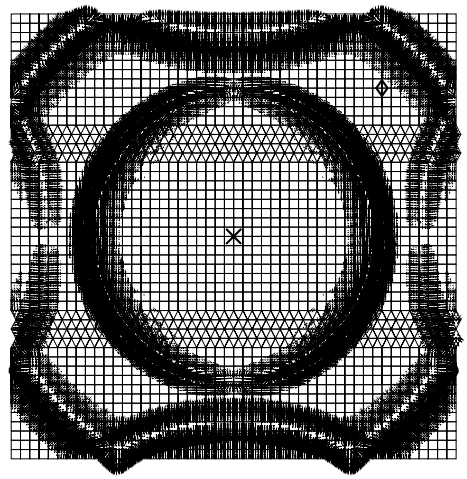

Fig. 3. Snapshot at time $t = 0.5$ s for a homogenous block of size 2400 m $\times$ 2400 m, with a vertical force source (indicated by the cross) located in its middle, at $x_s = 1200$ m and $z_s = 1200$ m, for the case of a mesh composed of quadrangles with four lines of triangles, with 48 elements in each direction of the grid. The direct P and S-waves can be clearly observed, as well as similar waves coming back from the edges of the model because of the periodic conditions. The receiver (indicated by the losange) located at $x_r = 2000$ m and $z_r = 2000$ m is used for a comparison to the analytical solution in Fig. 4.

able to compare the results to those obtained with quadrangles only, we use triangles of the same horizontal and vertical size as the quadrangles, thus having a base and a height of 50 m. This means that the triangles used are close to the optimal equilateral shape since the ratio of the length of their edges to the length of their base is $\sqrt{5}/2 \simeq 1.12$. The mesh with four lines of triangles is illustrated in Fig. 3, where a snapshot of the wavefronts is presented at time $t = 0.5$ s. The direct P and S-wavefronts generated by the vertical force can be clearly observed, as well as waves coming back from the edges of the grid due to the periodic conditions.

To quantify the numerical dispersion related to the use of triangles precisely, in Fig. 4 we compare the results to the analytical solution, at the same receiver as in Fig. 2 for quadrangles. We see that in the case of a mesh with quadrangles and four lines of triangles, the error remains small and is comparable in amplitude to that of Fig. 2 for quadrangles only, but more oscillations are present, in particular for waves that have traveled several times through the triangles, as can be seen between $t = 1.5$ s and $t = 2$ s. This effect is particularly clear for the mesh of triangles only, for which the oscillations are stronger, even for the direct S-wave around $t = 0.6$ s, and significant phase shifts are observed because of the numerical dispersion. This means that triangles are less accurate than quadrangles of the same size and induce more numerical dispersion. In the case of a mesh of only triangles, it is interesting to see how many elements we need to use to obtain an accuracy of the same order as that obtained using only quadrangles and 4.6 points per wavelength in Fig. 2. We therefore redo the simulation using 64 elements in each direction of the grid rather than 48. This corresponds to a mean value of 6.1 points per shortest S-wavelength instead of 4.6. A snapshot of the displacement vector is presented in Fig. 5 at time $t = 0.5$ s. The waves do

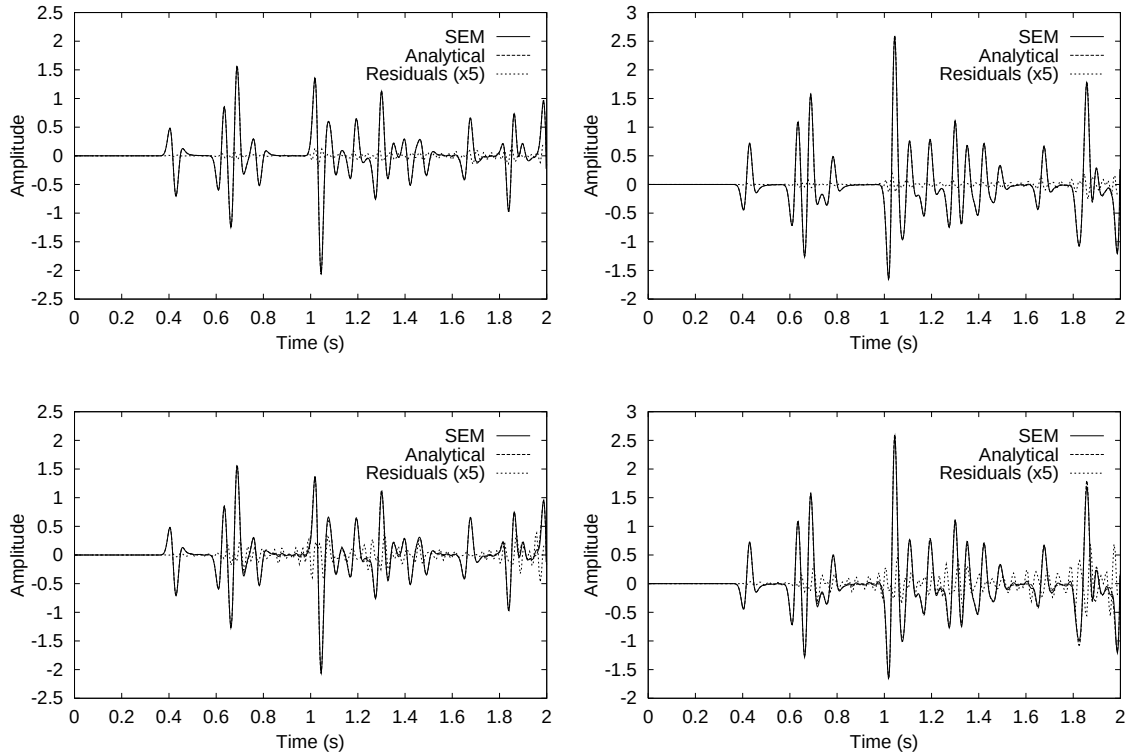

Fig. 4. Horizontal (left) and vertical (right) component of displacement (solid line) recorded at a receiver located at $x_r = 2000$ m and $z_r = 2000$ m, for a 2400 m $\times$ 2400 m block with a vertical force source located in its middle. With respect to Fig. 2, the medium is discretized using a mesh consisting of quadrangles with four lines of triangles (top), and triangles only (bottom), with 48 elements in each direction of the grid. The mesh with four lines of triangles, and a corresponding snapshot of the wavefield, are shown in Fig. 3. The polynomial degree used is $N = 5$. The analytical solution is also presented (dashed line) as well as the residuals between the two curves, amplified by a factor of five for clarity (dotted line). Significant numerical dispersion is observed, in particular for the direct S-wave around $t = 0.6$ s for the mesh with triangles only, and also for waves that have traveled several times through the grid because of the periodic conditions (after $t = 1$ s). Comparison with Fig. 2 clearly shows that triangles are less accurate than quadrangles of the same size.

not seem to exhibit any significant numerical dispersion, in particular the S-wavefront which has the shortest wavelength. To quantify this precisely, in Fig. 6 we show the displacement recorded at the same receiver as in Figs. 2 and 4. The error has been drastically reduced compared to Fig. 4, to a level comparable to that obtained with pure quadrangles in Fig. 2. A similar experiment, not presented here, conducted using 60 elements in each direction of the grid, i.e., using a mean value of 5.8 grid points per shortest S-wavelength, led to results that exhibited oscillations significantly bigger than in the reference of Fig. 2. From these two numerical experiments, we can conclude that the use of roughly 6 points per wavelength is necessary in the case of a discretization based upon triangles to obtain a level of accuracy similar to that obtained using 4.5 to 5 points in the case of classical quadrangles. This gives a numerical overhead ratio of roughly 1.20 to 1.35.

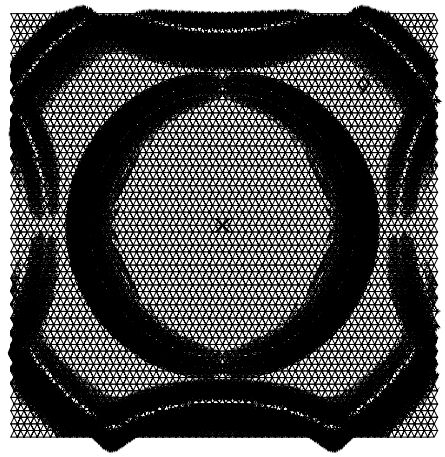

Fig. 5. Snapshot at time $t = 0.5$ s for a homogenous block of size 2400 m $\times$ 2400 m with a vertical force source located in its middle, for the case of a mesh composed of triangles only, with 64 elements in each direction of the grid. The direct P and S-waves can be clearly observed, as well as similar waves coming back from the edges of the model because of the periodic conditions. The wavefronts do not exhibit any significant numerical dispersion. The cross indicates the position of the source, and the losange shows the position of the receiver at which a comparison to the analytical solution is performed in Fig. 6.

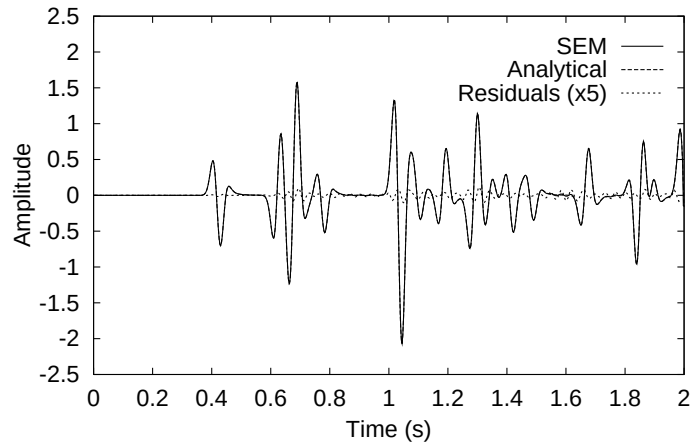

(a)

Fig. 6. Horizontal (a) and vertical (b) component of displacement (solid line) recorded at a receiver located at $x_r = 2000$ m and $z_r = 2000$ m, for a 2400 m $\times$ 2400 m block with a vertical force source located in its middle. With respect to Figs. 2 and 4, the medium is discretized using a mesh composed of triangles only, with 64 elements in each direction of the grid. The mesh and a corresponding snapshot of the wavefield are shown in Fig. 5. The polynomial degree used is $N = 5$. The analytical solution is also presented (dashed line) as well as the residuals between the two curves, amplified by a factor of five for clarity (dotted line). The numerical dispersion has been significantly reduced with respect to the results in Fig. 4 (bottom). We have reached a level of accuracy comparable to that obtained with a mesh of quadrangles only in Fig. 2.

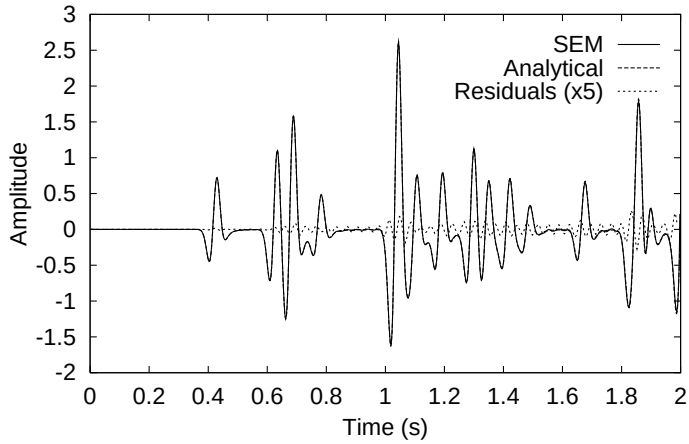

(b)

Fig. 6. (*Continued*)

6. Conclusions

We have shown that the use of a spectral element method based upon both quadrangles and triangles enables us to model wave propagation in 2-D elastic media accurately. The method, based on the classical Gauss–Lobatto–Legendre points in the quadrangles and on the Fekete points in the triangles, introduces more flexibility during the mesh generation step while keeping the most important properties of the classical spectral-element method, such as a global diagonal mass matrix.

Detailed numerical tests in a homogeneous medium and comparisons with both the analytical solution and the solution computed with only quadrangles, have illustrated that triangles are slightly less accurate than quadrangles. Using a polynomial degree $N = 5$, very good accuracy is obtained with quadrangles using roughly 4.5 to 5 grid points per wavelength, while to obtain a similar level of accuracy using triangles, roughly 6 points per wavelength are required. The use of more points per wavelength also implies a stronger restriction on the Courant stability condition of the explicit time scheme. On the triangles the so-called tensorisation of the classical spectral elements is lost, which implies that the number of operations necessary for computing a derivative is higher. This additional numerical cost is compensated by the much higher flexibility allowed by the use of two types of elements in the same mesh.

Acknowledgments

The authors would like to acknowledge the partial support provided by the David and Lucille Packard Foundation, NSF and NEHRP. They thank two anonymous reviewers for constructive comments that helped improve the manuscript.

References

1. J. Virieux, "*P-SV* wave propagation in heterogeneous media Velocity-stress finite-difference method," *Geophysics* **51**, 889 (1986).
2. R. W. Graves, "Simulating seismic wave propagation in 3D elastic media using staggered-grid finite differences," *Bull. Seis. Soc. Am.* **86**, 1091 (1996).
3. J. M. Carcione and P. J. Wang, "A Chebyshev collocation method for the wave equation in generalized coordinates," *Comp. Fluid Dyn. J.* **2**, 269 (1993).
4. E. Tessmer and D. Kosloff, "3-D elastic modeling with surface topography by a Chebyshev spectral method," *Geophysics* **59**, 464 (1994).
5. D. Komatitsch, F. Coutel, and P. Mora, "Tensorial formulation of the wave equation for modelling curved interfaces," *Geophys. J. Int.* **127** 156 (1996).
6. H. Bao, J. Bielak, O. Ghattas, L. F. Kallivokas, D. R. O'Hallaron, J. R. Shewchuk, and J. Xu, "Large-scale simulation of elastic wave propagation in heterogeneous media on parallel computers," *Comput. Methods Appl. Mech. Engrg.* **152**, 85 (1998).
7. G. Seriani, E. Priolo, J. M. Carcione, and E. Padovani, "High-order spectral element method for elastic wave modeling," in *Expanded Abstracts of the 62nd Soc. Expl. Geophys. Meeting* (SEG, Tulsa, Oklahoma, 1992), pp. 1285–1288.
8. E. Priolo, J. M. Carcione, and G. Seriani, "Numerical simulation of interface waves by high-order spectral modeling techniques," *J. Acoust. Soc. Am.* **95**, 681 (1994).
9. D. Komatitsch, "Méthodes spectrales et éléments spectraux pour l'équation de l'élastodynamique 2D et 3D en milieu hétérogène," Ph.D. Thesis, Institut de Physique du Globe, Paris, France, 1997.
10. E. Faccioli, F. Maggio, R. Paolucci, and A. Quarteroni, "2D and 3D elastic wave propagation by a pseudo-spectral domain decomposition method," *J. Seismology* **1**, 237 (1997).
11. D. Komatitsch and J. P. Vilotte, "The spectral element method: An efficient tool to simulate the seismic response of 2D and 3D geological structures," *Bull. Seis. Soc. Am.* **88**, 368 (1998).
12. D. Komatitsch and J. Tromp, "Introduction to the spectral-element method for 3-D seismic wave propagation," *Geophys. J. Int.* **139**, 806 (1999).
13. D. Komatitsch, C. Barnes, and J. Tromp, "Simulation of anisotropic wave propagation based upon a spectral element method," *Geophysics* **65**, 1251 (2000).
14. D. Komatitsch, C. Barnes, and J. Tromp, "Wave propagation near a fluid-solid interface: A spectral element approach," *Geophysics* **65**, 623 (2000).
15. M. A. Taylor, R. Loft, and J. Tribbia, "Performance of a spectral element atmospheric model (SEAM) on the HP Exemplar SPP2000," Technical Report NCAR/TN-439+EDD, (National Center for Atmospheric Research, Boulder, Colorado, 1998).
16. P. Moczo, E. Bystrický, J. Kristek, J. M. Carcione, and M. Bouchon, "Hybrid modeling of *P-SV* seismic motion at inhomogeneous viscoelastic topographic structures," *Bull. Seis. Soc. Am.* **87**, 1305 (1997).
17. D. J. P. Lahaye, F. Maggio, and A. Quarteroni, "Hybrid finite element-spectral element approximation of wave propagation problems," *East-West J. Numer. Math.* **5**, 265 (1997).
18. F. Casadei and E. Gabellini, "Implementation of a 3D coupled spectral element solver for wave propagation and soil-structure interaction simulations," Technical Report EUR17730EN, European Commission Joint Research Center, Ispra, Italy, 1997.
19. M. Dubiner, "Spectral methods on triangles and other domains," *J. Sci. Comp.* **6**, 345 (1993).
20. S. J. Sherwin and G. E. Karniadakis, "A triangular spectrial element method: Applications to the incompressible Navier-stokes equations," *Comput. Methods Appl. Mech. Engrg.* **123**, 189 (1995).

21. B. A. Wingate and J. P. Boyd, "Spectral element methods on triangles for geophysical fluid dynamics problems," in *Proc. Third International Conference on Spectral and High-order Methods*, eds. A. V. Ilin and L. R. Scott (Houston J. Mathematics, Houston, Texas, 1996), pp. 305–314.
22. Q. Chen and I. Babuška, "Approximate optimal points for polynomial interpolation of real functions in an interval and in a triangle," *Comput. Methods Appl. Mech. Engrg.* **128**, 405 (1995).
23. M. A. Taylor and B. A. Wingate, "The Fekete collocation points for triangular spectral elements," *SIAM J. Numer. Anal.*, in press (2000).
24. M. A. Taylor and B. A. Wingate, "A generalized diagonal mass matrix spectral element method for non-quadrilateral elements," *Appl. Num. Math.* **33**, 259 (2000).
25. T. J. R. Hughes, *The Finite Element Method, Linear Static and Dynamic Finite Element Analysis* (Prentice-Hall, Englewood Cliffs, NJ, 1987).
26. C. Canuto, M. Y. Hussaini, A. Quarteroni, and T. A. Zang, *Spectral Methods in Fluid Dynamics* (Springer-Verlag, New York, 1988).
27. J. Lyness and R. Cools, "A survey of numerical cubature over triangles," *Proc. Symposia in Applied Mathematics* **48**, 127 (1994).
28. J. S. Hesthaven, "From electrostatics to almost optimal nodal sets for polynomial interpolation in a simplex," *SIAM J. Numer. Anal.* **35**, 655 (1998).
29. Q. Chen and I. Babuška, "The optimal symmetrical points for polynomial interpolation of real functions in the tetrahedron," *Comput. Methods Appl. Mech. Engrg.* **137**, 89 (1996).
30. J. S. Hesthaven and C. H. Teng, "Stable spectral methods on tetrahedral elements," *SIAM J. Sci. Comput.* **21**, 2352 (2000).
31. L. Fejér, "Bestimmung derjenigen Abszissen eines Intervalles für welche die Quadratsumme der Grund-funktionen der Lagrangeschen Interpolation in Intervalle[-1, 1] ein möglichst kleines Maximum besitzt," *Ann. Scuola Norm. Sup. Pisa Sci. Fis. Mt. Ser. II* **1**, 263 (1932).
32. L. Bos, personal communication (1998).
33. L. Bos, "On certain configurations of points in $\mathbb{R}^n$ which are unisolvent for polynomial interpolation," *J. Approx. Theory* **64**, 271 (1991).
34. R. A. Horn and C. R. Johnson, *Matrix Analysis* (Cambridge University Press, Cambridge, 1985).
35. M. Baran, "Complex equilibrium measure and Bernstein type theorems for compact sets in $\mathbb{R}^n$," *Proc. Amer. Math. Soc.* **123**, 485 (1994).
36. W. L. Pilant, *Elastic Waves in the Earth* (Elsevier, Amsterdam, 1979).
37. N. Tarnow and J. C. Simo, "How to render second-order accurate time-stepping algorithms fourth-order accurate while retaining the stability and conservation properties," *Comput. Methods Appl. Mech. Engrg.* **115**, 233 (1994).